HHS Public Access

Author manuscript

ACS Nano. Author manuscript; available in PMC 2022 December 28.

Published in final edited form as:

ACS Nano. 2021 December 28; 15(12): 20504–20516. doi:10.1021/acsnano.1c09064.

Targeting the Extracellular Matrix in Traumatic Brain Injury Increases Signal Generation from an Activity-Based Nanosensor

Rebecca M. Kandell[‡], **Julia A. Kudryashev**[‡], **Ester J. Kwon**[*]

Department of Bioengineering, University of California, San Diego, La Jolla, California 92093, United States

Abstract

Traumatic brain injury (TBI) is a critical public health concern and major contributor to death and long-term disability. After the initial trauma, a sustained secondary injury involving a complex continuum of pathophysiology unfolds, ultimately leading to the destruction of nervous tissue. One disease hallmark of TBI is ectopic protease activity, which can mediate cell death, extracellular matrix breakdown and inflammation. We previously engineered a fluorogenic activity-based nanosensor for TBI (TBI-ABN) that passively accumulates into the injured brain across disrupted vasculature and generates fluorescent signal in response to calpain-1 cleavage, thus enabling *in situ* visualization of TBI-associated calpain-1 protease activity. In this work, we hypothesized that active targeting to the extracellular matrix of the injured brain would improve nanosensor accumulation in injured brain beyond passive delivery alone and lead to increased nanosensor activation. We evaluated several peptides that bind exposed/enriched ECM constituents in the brain and discovered that nanomaterials modified with peptides that target hyaluronic acid (HA) displayed widespread distribution across the injury lesion, in particular colocalizing with perilesional and hippocampal neurons. Modifying TBI-ABN with HA-targeting peptide led to increases in activation in a ligand valency-dependent manner, up to 6.6-fold in the injured cortex compared to non-targeted nanosensor. This robust nanosensor activation enabled 3D visualization of injury-specific protease activity in a cleared and intact brain. In our work, we establish that targeting brain ECM with peptide ligands can be leveraged to improve the distribution and function of a bioresponsive imaging nanomaterial.

Graphical Abstract

[*]Corresponding author. ejkwon@ucsd.edu.

Author Contributions

The manuscript was written through contributions of all authors. All authors have given approval to the final version of the manuscript.

[‡]These authors contributed equally.

Supporting Information. The following files are available free of charge. Supplementary Tables 1–2 and Figures 1–10: table of immunostaining reagents, table of concentration measurements for calpain substrate peptide, blood half-life of ECM-targeted nanomaterials, triplicate histology of ECM-targeted nanomaterials, representative brains with alternative anti-FAM antibody, maximal cleavage velocities of TBI-ABNs, raw signal from TBI-ABN activation in brain lysates for each mouse in the triplicate, TBI-ABN fold-change in activation for off-target organs, triplicate histology of nanosensor activation, CUBIC clearing progress for brains, LSFM horizontal cross-sections across imaging depths, 3D clipping planes (PDF).

Supplementary Video: Video showing 3D nanosensor localization and activation in the CUBIC-cleared injured brain (MP4)

The authors declare no competing financial interest.

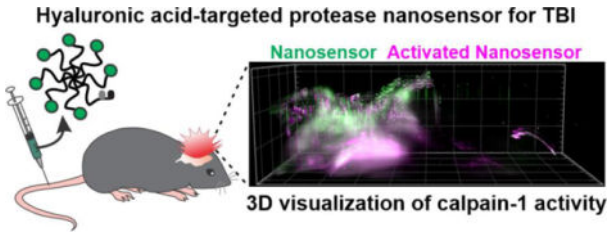

Keywords

hyaluronic acid; controlled cortical impact; calpain-1; peptides; protease activity; light sheet microscopy; CUBIC

Traumatic brain injury (TBI) affects over 1.5 million Americans per year and an estimated 3.17 million patients live with chronic neurodisability due to TBI.[1,2] After the primary injury, a progressive secondary injury unfolds within the brain over the course of hours to months caused by a complex continuum of pathophysiology characterized by hallmarks such as neuronal apoptosis, excitotoxicity, inflammation, and blood-brain barrier (BBB) dysfunction.[3] One signature of secondary injury pathophysiology is ectopic protease activity; for instance, the calcium-dependent cysteine protease calpain-1 cleaves cytoskeletal proteins and contributes to apoptotic and necrotic cell death,[4] and its activity is correlated with worsened TBI outcome.[5–7] Protease activity measurements have the potential to improve understanding of TBI disease biology and can serve as clinical biomarkers for disease progression,[8,9] but there are few approaches to measure protease activity in the living brain. In order to measure TBI-associated calpain-1 activity, we previously engineered a fluorogenic activity-based nanosensor for TBI (TBI-ABN) comprised of a Förster resonance energy transfer (FRET)-based peptide substrate of calpain-1 conjugated to a polymeric nanomaterial scaffold.[10] When administered intravenously in a TBI mouse model, we demonstrated that TBI-ABN could accumulate into injured brain tissue and activate in the context of injury. To sample ectopic protease activity in the injured tissue, this technology relied on size-dependent accumulation in brain tissue *via* transient BBB permeability, a hallmark of TBI pathophysiology. This passive accumulation of nanomaterials localized to diseased tissue has been called an “enhanced permeation and retention” (EPR)-like effect,[11,12] and a similar phenomenon is described in other diseases such as cancer,[13,14] arthritis,[15] and myocardial infarction.[16,17] However in TBI, reliance on passive targeting alone is generally limited because unlike chronic conditions such as cancer and arthritis, BBB disruption after TBI is transient, restricting the time window for nanomaterial delivery to hours after injury.[11,18] Furthermore, increased intracranial pressure from ischemia-associated edema creates a pressure gradient that likely limits nanomaterial diffusion across the extracellular space (ECS).[19] Thus, strategies to control the tissue-level distribution of activity-based nanosensors beyond passive targeting have the potential to increase protease-specific signal generation and therefore increase the sensitivity of nanosensors, as was previously demonstrated when the addition of tumor-targeting ligands to an MMP-9-sensitive ABN enabled ultrasensitive detection of low tumor burdens in a urinary readout.[20]

As a complementary approach in addition to passive delivery, active targeting *via* peptide or protein affinity ligands (*e.g.*, transferrin,[21,22] HER2 antibodies,[23,24] RVG,[18,25], Lyp-1[26,27]) can improve the transport and/or tissue-level distribution of payloads. The extracellular matrix (ECM) represents an attractive biological target for nanomaterials due to its abundance and high density of binding moieties,[28] and therefore has the potential to act as a binding reservoir for exogenously delivered nanomaterials. Active targeting to ECM has been successfully applied to nanoparticle and protein therapeutics within the contexts of cancer[29–32] and arthritis-associated inflammation.[33,34] The dysregulated vasculature associated with cancer and inflammation exposes tissue ECM to materials in systemic circulation. In addition, aberrantly deposited ECM constituents can serve as disease-specific "neo-antigens" to improve distribution and efficacy of therapeutics. For example, the fusion of a collagen binding domain to chemokine CCL4 increased the accumulation of systemically administered CCL4 within collagen-rich tumors, leading to an enhancement of intra-tumor infiltration of immune cells when used in combination with checkpoint inhibitor immunotherapy.[32] In the brain, tissue is largely inaccessible to systemically administered synthetic nanomaterials under physiological conditions due to the selective and tightly regulated BBB. After TBI, transient BBB disruption initiated by the injury enables access to brain parenchyma,[10,11,18,35] including the ECM. In addition, the composition of ECM in the brain is distinct from that of peripheral organs; the brain is enriched with hyaluronic acid (HA) and sulfate proteoglycans, while fibrillar collagens and elastin are less represented.[36,37] This composition is furthermore changed in disease, with tenascins, laminin, chondroitin sulfate proteoglycans and heparin sulfate proteoglycans focally upregulated in the TBI lesion.[36,37] Local levels of HA are also perturbed due to changes in HA metabolism; hyaluronidases can degrade HA into bioactive fragments,[36,38] and expression of hyaluronic acid synthases are increased after experimental brain injury.[38] In addition to the tissue ECM present in the brain parenchyma, vascular injury leads to fibrin deposition during natural clotting and transient exposure of collagen IV in the basement membrane.[36] Each of these brain ECM components are potential targets for nanomaterials in the context of TBI. The approach of targeting the ECM after brain injury is highlighted by the recent identification of TBI-specific peptides *via in vivo* phage display.[39] This unbiased screening approach against whole brain tissue after TBI identified a peptide CAQK, whose receptors were discovered to be upregulated tenascin and versican proteoglycans in the ECM. CAQK modification enhanced the accumulation, acute retention, and activity of nanomaterials carrying siRNA payloads in a penetrating brain injury model.[39] Beyond this demonstration, active targeting to the ECM after TBI has been largely unexplored.

In this manuscript, we hypothesized that actively targeting nanomaterials to the brain ECM can increase the bioavailability and therefore activity of a diagnostic payload after systemic delivery in a TBI mouse model. We first performed an *in vivo* evaluation of nanomaterials modified with a selection of peptides that target major brain ECM constituents: proteoglycans, collagen IV, fibrin, and HA. In a controlled cortical impact (CCI) model of TBI in mice, nanomaterials modified with peptides that targeted HA led to widespread distribution across cortical and hippocampal perilesional tissue after intravenous administration, and tissue localization was distinct from nanomaterials modified with peptides that targeted other ECM components. To determine whether this ECM-targeting-

mediated change in tissue distribution could be harnessed into a functional outcome, we added HA-targeting to TBI-ABN, a nanosensor that activates in response to calpain-1 protease activity. We modified TBI-ABNs with HA-targeting peptide at various levels of substitutions, quantified calpain-1 nanosensor activation in injured brain tissue, and observed that targeting could increase activation up to 6.6-fold over non-targeted nanosensor, which suggests that increasing nanomaterial avidity to the ECM translates into enhanced nanosensor sensitivity. At the tissue level, we observed that the activation of HA-targeted TBI-ABN throughout the perilesional brain tissue colocalized with both neuronal and endothelial cell populations. Finally, light sheet imaging of TBI-ABN in cleared brain revealed nanosensor activation in proximity to the impact lesion in both the hippocampus and cortex. In summary, we establish that targeting an activity-based nanosensor to the brain ECM can significantly increase signal generation when applied to an animal model of TBI after systemic administration, enabling tissue-level visualization of aberrant calpain-1 protease activity in the injured brain.

RESULTS & DISCUSSION

Nanomaterials targeted to hyaluronic acid have widespread distribution in the injured brain.

In order to generate nanomaterials that interact with the brain ECM after intravenous delivery, we first identified peptide ligands from literature that bind to ECM constituents that are either exposed or enriched in the injured brain.[36] The selected ECM targets and ligand sequences were proteoglycans (CAQK),[39] collagen IV (KLWVLPK),[40] fibrin (CREKA),[41] and hyaluronic acid (STMMSRSHKTRSHHV).[42,43] Throughout the manuscript, these ECM-targeting peptides are referred to as PGpep, CIVpep, FIBpep, and HApep, respectively. These peptides are low molecular weight, linear sequences with comparable physicochemical properties (Table 1). In previous work, we have established that the physiochemical properties of peptides influence nanoparticle pharmacokinetics in a mouse model of TBI.[44] Our nanomaterial scaffold was a 40 kDa 8-arm polyethylene glycol (PEG) which was selected for several reasons. First, each arm can participate in chemical conjugation, thus allowing for multivalent ligand presentation. Second, we previously established that its ~10 nm hydrodynamic diameter facilitates accumulation in the injured brain after intravenous administration[10] since it is larger than the ~5.5 nm renal filtration limit which prevents rapid kidney excretion,[45] yet smaller than the pores in the ECS which allows for diffusion into brain tissue.[19,46] Third, PEG is a component used to extend *in vivo* circulation half-life in multiple FDA-approved formulations.[47] The ECM-targeting peptides were synthesized with the fluorescent molecule fluorescein (FAM) for quantification and a cysteine for reaction with maleimides on the 8-arm PEG. The PEG scaffold was reacted with one mole equivalence of fluorescent molecule VivoTag S-750 (VivoTag 750) and the remaining moieties were fully reacted with ECM-targeting peptides. The FAM on the peptide was utilized for quantitative biodistribution and histology and VivoTag 750 on the PEG scaffold was utilized for near-infrared surface imaging of organs. A non-targeted nanomaterial control was synthesized by modifying PEG with cysteine (Cys) instead of ECM-targeting peptide. In addition, the linear form of the well-studied peptide

RGD[48] was included as a control due to the known elevation of integrin expression in inflammation.[49–51]

We evaluated the biodistribution of nanomaterials modified with each ECM-targeting peptide after intravenous delivery in a controlled cortical impact (CCI) mouse model of TBI (Figure 1A). CCI is a well-established model of TBI that has reproducible molecular phenotypes,[52] including elevation of calpain-1 activity.[10,53] Injuries were created by performing a 5 mm craniotomy over the right hemisphere of the brain and impacting the exposed dura with an electromagnetically-driven probe 2 mm in diameter at a speed of 3 m/s and depth of 2 mm. ECM-targeting peptide-modified PEG nanomaterial (25 nmoles of peptide per injection based on FAM absorbance, corresponding to a dosage range of 1136–1389 nmol/kg) was injected intravenously 6 hours post-CCI and mice were perfused and organs harvested 1 hour post-injection, an experimental timeline established by previous work.[39] Surface imaging of the VivoTag 750 label in intact organs shows that nanomaterial accumulation in the brain was localized to the injured brain hemisphere (Figure 1B). This accumulation of intravenously delivered nanomaterials into the injured hemisphere due to local, transient permeability of the dysregulated blood-brain barrier is consistent with previous work from our group[10,18,44] and others.[11,12] Nanomaterials modified with CIVpep had high liver accumulation over all other materials. One potential hypothesis for this observation is the abundance of collagens I, III, IV, and V in the basement membrane of the liver.[54] We also observed significant nanomaterial accumulation in the kidneys, in particular for FIBpep- and PGpep-modified nanomaterials.

While surface imaging gives spatial distribution within an organ, it is limited by imaging depth and we therefore performed a bulk analysis of homogenized organs to quantify nanomaterial accumulation. Bulk quantitative biodistribution analysis was based on fluorescence signal from the FAM label on the peptide which was used to calculate the percent injected dose per gram tissue (%ID/g tissue) from a standard of known peptide concentrations. We observed that bulk quantitative analysis was largely consistent with surface imaging (Figure 1C). CIVpep-modified nanomaterials significantly accumulated in the liver over all nanomaterials modified with other ECM peptides (between 8.9-fold and 24.8-fold). Moreover, nanomaterials modified with PGpep and FIBpep had the highest overall kidney accumulation, followed by RGD. The ECM-targeting peptides did not appear to have significant impacts on total accumulation in the injured brain (%ID/g between 0.80 and 1.68), consistent with previous observations that targeting has modest effects on total tissue accumulation.[21,22,24,26] Considering that the targeting peptides we investigated bind to the ECM, we posit that nanomaterials must first encounter the ECM through passive targeting and therefore ECM-targeting peptides would be unlikely to contribute to changes in total brain accumulation. This is further corroborated by similar blood half-lives measured for each ECM-targeted nanomaterial (Figure S1); previous work has established that passive accumulation after systemic administration correlates with blood half-life due to a maintenance of a concentration gradient of nanomaterials between the blood and target tissue.[55]

To investigate the spatial distribution of nanomaterials in the injured brain at greater depth and resolution than could be achieved with surface imaging, we completed a qualitative

comparison of nanomaterial distribution in brain sections following immunostaining with an anti-FAM antibody (Figure 1D, Table S1). We observed a marked increase in the distribution of HApep-modified nanomaterials in the injured area of the brain compared to the other peptide-modified nanomaterials. This observation was consistent across triplicate brains (Figure S2). To verify that the FAM-immunostaining was specific, we used an alternate anti-FAM antibody and observed the same outcome (Figure S3). The non-targeted nanomaterial served as a negative control for non-specific staining since no FAM was present on that nanomaterial. The widespread distribution of HApep-modified nanomaterial in the tissue proximal to the injury was observed despite the lack of appreciable differences measured in bulk analysis of FAM signal. This may be due to the reduced sensitivity of measurement in the bulk analysis since antibody staining was used to image nanomaterial in brain sections. In addition, analysis of brain sections revealed that nanomaterial was largely restricted to the cortical and hippocampal tissue in close proximity to the injury, whereas in bulk quantification the whole hemisphere was homogenized potentially diluting total nanomaterial signal. Our results were also consistent with previous studies that establish active targeting has greater impacts on intra-tissue distribution of nanoparticles over bulk accumulation.[22]

Hyaluronic acid-targeted nanomaterial accumulates within injured brain tissue and colocalizes with hippocampal and cortical neurons.

Having demonstrated that nanomaterials modified with peptides that target HA have improved distribution within the injured brain over peptides that target other ECM components, we sought to further characterize the tissue-level distribution of this nanomaterial. We stained and imaged both the uninjured contralateral and injured ipsilateral hemispheres in coronal brain sections and observed that nanomaterial localization is specific to the injured hemisphere with minimal signal in the uninjured hemisphere (Figure 2A), consistent with our previous observation (Figure 1B). Nanomaterial accumulation coincided with areas of tissue trauma in the right hemisphere, where the CCI was applied. Within the injury, there was significant nanomaterial signal in the perilesional cortical and hippocampal regions.

Next, to identify nanomaterial localization around brain cells of interest, we performed immunostaining for neurons — a major source of calpain-1[56,57] and the cellular target for neuroprotective therapeutics.[58] HApep-modified nanomaterial was found to colocalize with subsets of both cortical and hippocampal neurons (Figure 2B). In the perilesional cortex (Figure 2Bi), nanomaterial localized to neurons adjacent to tissue trauma and similarly, nanomaterial localized to neurons in the hippocampal region (Figure 2Bii).

We next compared the localization of our HA-targeted nanomaterial to the spatial distribution of endogenous HA. A biotinylated hyaluronic acid binding protein (bHABP) was used to visualize native HA, as described previously.[59–62] Consistent with published literature,[60–62] regions with HABP binding were enriched in the hippocampus and cerebral cortex (Figure 2C). The staining of bHABP in both the cortex (Figure 2Ci) and hippocampus (Figure 2Cii) was mainly diffuse, although enrichment was observed around the cell bodies of hippocampal neurons and select neurons in the cortex. This observation is consistent

with literature, as HA is a known component of perineuronal nets (PNNs) that surround neuronal cell bodies.[60] In some instances, our HA-targeted nanomaterial colocalized with cells with HABP perineuronal staining in both the cortex and hippocampus (Figure 2Ci–ii, arrows). Differences observed between the distribution of HABP staining of brain slices and systemic administration of HApep-modified nanomaterial are likely due to limited access of intravenously administered nanomaterial across the damaged vasculature and extracellular space.[19,46] Additionally, there are likely differences between the specificity of HABP and the short peptide ligand HApep since the modes of discovery and composition are divergent.[42,59]

Targeting hyaluronic acid enhances the *in vivo* sensitivity of an activity based nanosensor for TBI (TBI-ABN).

We previously developed an activity based nanosensor for TBI (TBI-ABN) for detection of calpain-1 protease activity in a mouse model of TBI.[10] The TBI-ABN consists of a FRET pair (fluorophore: Cy5, quencher: QSY21) separated by the calpain-1-cleavable peptide sequence QEVYGAMP, which is derived from a native calpain-1 substrate, αII-spectrin,[63] attached to 40 kDa 8-arm PEG, the same polymeric scaffold that we used to evaluate brain ECM-targeting peptides (Figure 1). When active calpain-1 protease is present, the FRET substrate on TBI-ABN is cleaved, leading to dequenching of Cy5 fluorescence. We previously demonstrated that TBI-ABN could passively accumulate in the injured brain and generate fluorescent signal in response to locally activated calpain-1 after systemic administration in CCI-injured mice.[10] As a demonstration that spatial localization in the TBI microenvironment can increase the activity of nanomaterials, we proposed that the addition of active targeting ligands would improve signal generation from TBI-ABN. We previously established that the addition of tumor targeting increased the sensitivity of an activity-based protease nanosensor for cancer *via in silico* and experimental analyses.[20] In the context of TBI, we hypothesized that the incorporation of HA targeting in our TBI-ABN design would increase nanosensor activation since HA-targeted nanomaterial colocalized within perilesional cortical and hippocampal neurons (Figure 2), and neurons are a major cellular source of calpain-1.[56,57]

We synthesized TBI-ABNs with varying degrees of HA targeting in order to investigate the relationship between ligand valency and TBI-ABN activation *in vivo*. This was motivated by the phenomenon that multivalent molecular interactions confer enhanced overall binding strength (*i.e.*, avidity) and increase the likelihood for binding events to occur.[64] Previous studies have established the importance of tuning binding avidity for nanomaterial targeting; for example, increasing densities of transferrin targeting ligand on gold nanoparticles led to an increase in nanoparticle localization in tumor cells, although higher ligand density also increased off-target uptake by hepatocytes.[22] In order to create TBI-ABNs with matched amount of calpain-1 FRET substrate peptide and varying levels of targeting for comparison studies, a 1:1 stoichiometry of calpain FRET substrate and 8-arm PEG was reacted, split into three parts, and HApep added at stoichiometric ratios of 0, 4, and 7 to yield non-targeted, moderate-targeted, and high-targeted TBI-ABNs respectively (Figure 3A). Absorbance measurements verified that stoichiometric ratios of HApep to calpain FRET peptide on the TBI-ABN were 0, ~3.2, ~8.5 for non-, moderate- and high-

targeted TBI-ABNS respectively (Table S2). In order to verify that HApep modification of TBI-ABN did not significantly impact nanosensor performance, non-, moderate-, and high-targeted TBI-ABNs were incubated with human calpain-1 enzyme at various concentrations to construct Michaelis-Menten kinetics curves. Maximum cleavage velocities for non-, moderate-, and high-targeted TBI-ABNs were 120.0 RFU/min, 73.72 RFU/min, and 76.13 RFU/min respectively, indicating that the incorporation of HApep moderately decreased calpain-1 cleavage kinetics of TBI-ABN (Figure 3B). A similar decrease in cleavage kinetics was observed when non-targeted TBI-ABNs were mixed with unconjugated HApep in molar ratios matching the moderate- and high-targeted TBI-ABNs, indicating that the presence of HApep independent of conjugation led to modest decreases in calpain-1 cleavage kinetics (Figure S4).

Next, we quantified TBI-ABN activation after intravenous administration in a mouse model of TBI. Non-, moderate-, and high-targeted nanosensors were administered *via* tail-vein at matched calpain-1 FRET substrate concentrations three hours after CCI, a time point when calpain-1 activation was measured to be locally increased in injured brain tissue.[10] One hour after nanosensor administration, fresh perilesional tissue and corresponding uninjured tissue from the contralateral hemisphere were collected and homogenized for bulk fluorescence analysis of dequenched FRET substrate from the TBI-ABN. Consistent with our previous observations, nanosensor activation was significantly greater in homogenate isolated from the injured hemisphere over the uninjured contralateral hemisphere by 6.2-fold, 8.1-fold, and 12.5-fold for non-, moderate-, and high-targeted TBI-ABNs respectively (Figure 3C). Comparing signal generation in the injured hemisphere across degrees of targeting, moderate and high targeting increased the levels of activated nanosensor signal by approximately 2.8-fold and 6.6-fold, respectively, over the non-targeted control. This increase in signal generation was observed despite the moderately decreased cleavage kinetics of HApep-modified TBI-ABNs measured *in vitro* with human calpain-1 enzyme (Figure 3B). Furthermore, Cy5 signal from activated nanosensor was greater than vehicle control and consistent across triplicate mice within each group (Figure S5). These results demonstrate that targeting TBI-ABN to the ECM increases activation within the injured brain in a valency-dependent manner. Although the high-targeted TBI-ABNs resulted in the highest overall signal in the brain, we also observed a concomitant increase in sensor activation in off-target organs compared to moderate- and non-targeted TBI-ABNs (Figure S6), suggesting that a moderate level of targeting may be desirable to achieve higher specificity of brain-to-off-target organ signal generation.

Targeting hyaluronic acid enables widespread TBI-ABN activation in injured brain tissue.

Having established that HApep modification of TBI-ABNs leads to an increase in bulk nanosensor activation in homogenized tissue lysate, we then set out to establish spatial activation of TBI-ABN in the injured brain tissue. The same experimental paradigm was repeated in triplicate, and coronal brain sections were imaged for activated nanosensor *via* dequenched Cy5 signal and nanosensor localization *via* the FAM label on HApep. We observed distinct nanosensor activation in all three HApep modification levels (non-, moderate-, and high-targeted) compared to the vehicle control (Figure 4), consistent with previous work.[10] In mice administered TBI-ABN with moderate or high HApep valency,

there was an observable increase in both nanosensor distribution within the injured cortex and nanosensor activation. The nanosensor tissue distribution resembled that of HApep nanomaterial (Figure 2) with accumulation in both the perilesional cortex and hippocampus, indicating the FRET substrate did not have a large impact on distribution, as expected with the low stoichiometry modification (Figure 4). The pattern of nanosensor activation in the perilesional cortex and hippocampus were consistent across triplicate brains within each group, although one brain with high-targeting had significantly increased signal generation compared to replicates in the same group (Figure S7). We note that the pattern of nanosensor distribution was distinct from the pattern of nanosensor activation, indicating some level of specificity of nanosensor activation. Overall, the brain sections reflected quantitative measurements made in bulk homogenates (Figure 3) and further supported our conclusion that incorporation of HA-targeting ligands increased nanosensor activation in the brain compared to non-targeted control. Since the high-targeted TBI-ABN yielded the maximal fold-increase of nanosensor activation in the brain, subsequent studies were performed with this nanomaterial.

Next, we investigated the distribution of activated TBI-ABN within the brain's cellular milieu because understanding the cellular localization of proteolytic activity could offer insight into TBI pathophysiology. Neurons are a major source of calpain-1 in the brain[56,57] and we have established that HA-targeted nanomaterial predominantly accumulates within cortical and hippocampal neurons proximal to the injury (Figure 2). Furthermore, endothelial cells can also contribute to abnormal calpain activation[65,66] and we expected nanosensor to have access to endothelial cells due to the vascular administration route.[10] We therefore investigated the activation of HA-targeted TBI-ABN in the context of neuronal and endothelial cell staining (Figure 5). In the perilesional cortex (Figure 5A), activated nanosensor signal colocalized with $NeuN^+$ neurons and $CD31^+$ endothelial cells. In the hippocampus (Figure 5B), activated nanosensor colocalized mainly with neurons, consistent with HA-targeted nanomaterial accumulation. Importantly, activation of nanosensor was distinct from the presence of nanosensor imaged by the FAM label on HApep in both $NeuN^+$ neurons and $CD31^+$ endothelial cells. Interestingly, the pattern of TBI-ABN activation in perilesional hippocampal and cortical neurons that we observed in our study was accordant with the pattern of neurodegeneration observed in previous studies that stained for degenerating neurons up to ~1 week after injury.[53,67]

The robust activation of HA-targeted TBI-ABN enabled the capture of macroscopic 3D spatial heterogeneity of protease activation across the TBI lesion in intact brains. We performed whole brain tissue clearing after TBI-ABN administration in CCI-injured mice with CUBIC (Clear, Unobstructed Brain/Body Imaging Cocktails and Computational analysis),[68] which enabled removal of light scattering components while matching the brain refraction index to the imaging media (Figure 6A, Figure S8). Cleared brains were imaged with light sheet fluorescence microscopy (LSFM) for TBI-ABN localization and activation (Figure 6B–C). The imaged volume was a 9.7 × 4.5 × 3.3 mm rectangular prism that encompassed the injured and contralateral cortices. A 3D rendering was generated of both TBI-ABN localization and activation based on the fluorescence of FAM on HApep and Cy5 on the dequenched FRET substrate, respectively (Figure 6B, Supplemental Video). Robust nanosensor activation was observed in the perilesional cortex in all directions from the

injury lesion, approximately 2 mm away from the injury epicenter, and in the hippocampal formation directly below the injury. A cylindrical pattern of nanosensor activation around the impact epicenter was observed, as demonstrated by horizontal cross sections at three optical sectioning depths (Figure S9). Furthermore, cross-sectional views of the injury (Figure 6C), generated using sagittal, horizontal, and coronal clipping planes (Figure S10), demonstrated that robust sensor activation was confined to the area proximal to the injury with minimal nanosensor activation detected in the contralateral hemisphere. Our 3D imaging corroborated the injury-specific activation observed in 2D imaging from brain sections (Figures 4–5). Overall, volumetric optical sectioning of cleared brains enabled spatial visualization of activated nanosensor, showing the extent of calpain-1 protease activity in relation to the injury.

CONCLUSIONS

Aberrant protease activity is linked to a worsening of TBI pathophysiology and prognosis[5–7] and tools to measure protease activity in the injured brain would allow for greater understanding of TBI progression. In this manuscript, the addition of HA-targeting peptides to a previously developed activity-based nanosensor for TBI[10] led to a robust signal that enabled visualization of protease activity in an intact brain. The HA-targeting peptide,[42] which is reported to have a dissociation constant between ~0.1–10 μM depending on HA length,[42,43] was selected following an *in vivo* screen of ECM-binding peptides. We observed that the addition of HA-targeting peptide increased TBI-ABN activation in a valency-dependent manner, consistent with observations that avidity strengthens with increasing peptide valency.[64] Beyond nanosensors, our results provide impetus to apply ECM targeting as a generalizable strategy to improve nanomaterial distribution and function within the injured brain after systemic administration.

Activity-based nanosensors are useful tools to probe protease activity in various disease states and can thus serve as imaging tools or biomarkers for diagnosis and prognosis.[8,9] We have shown that active targeting to brain ECM is a viable method to improve bioavailability of our nanosensor in the brain post-TBI, and thus increase both protease-dependent signal generation and sensitivity. Beyond improvements in sensitivity, the TBI-ABN design can incorporate the measurement of multiple proteases to further specify TBI-associated protease activity. Multiplexed detection of several disease-specific proteases has enhanced diagnostic specificity of urinary nano-reporters for lung[69] and prostate cancer.[70] In TBI, MMP-9 is a possible candidate for multiplexing as MMP-9 levels are elevated in patients post-TBI, and MMP-9 is implicated in BBB permeability.[71] Tethering substrates for multiple proteases onto a single nanomaterial scaffold and visualization in 3D would allow for the study of spatial activation of proteases in relation to each other; for example, calpain-1 has been shown to activate MMP-9 in TBI[72] and stroke.[73] In the future, the TBI-ABN platform could be re-designed for *in vivo* measurements with quenchable quantum dots[74] and tissue-penetrating near infrared optical imaging through cranial windows, or with superparamagnetic iron oxide nanoparticles[75] and magnetic resonance imaging (MRI). Furthermore, HA-targeting has the potential to be applied to a greater range of nanomaterials, including therapeutic nanomaterials. Our observation that HA-targeted nanomaterial colocalized with hippocampal and perilesional neurons provides

motivation for its use in the delivery of neuroprotective agents, since neuronal apoptosis is a hallmark of secondary injury and hippocampal neurodegeneration is associated with memory deficits after TBI.[76]

METHODS

Synthesis of ECM-targeted and TBI-ABN Poly(ethylene glycol) (PEG) Conjugates.

The following targeting peptides were synthesized by Lifetein (Somerset, NJ): PGpep (X(FAM)-CAQK), CIVpep (KLWVLPKGG-K(FAM)-GGC), FIBpep (X(FAM)-CREKA), HApep (X(FAM)-CSTMMSRSHKTRSHHV), and RGD (X(FAM)-CRGD). Calpain substrate FRET peptide (QSY21-QEVYGAMP-K(Cy5)-PEG2-GC-NH2) was synthesized by CPC Scientific Inc. (Sunnyvale, CA). X stands for 6-aminocaproic acid and PEG2 stands for poly(ethylene glycol). The 40kDa 8-arm PEG maleimide (tripentaerythritol) was purchased from Jenkem Technology (Beijing, China). For ECM-targeting peptide screening: PEG maleimide was batch reacted with 1 mol L-cysteine-functionalized VivoTag S-750 (PerkinElmer, Boston, MA). The reaction was then split to ensure matched VivoTag 750 modification for each conjugate and reacted with 8.4 mol equivalencies of each ECM-targeting peptide followed by quenching with an excess of L-cysteine. For HA-targeted TBI-ABNs: 8-arm PEG maleimide was batch reacted with 1 mol equivalent of calpain substrate FRET peptide, split and reacted with 0 mol (non-targeted), 4 mol (moderate targeting), or 8.4 mol (high targeting) equivalents of HApep in the presence of 50 mM triethylamine (TEA), then quenched with an excess of L-cysteine. All conjugates were dialyzed with water, and final concentrations were determined by absorbance of VivoTag 750, FAM, or Cy5 using a Spark multimode microplate reader (Tecan Trading AG, Switzerland).

Controlled Cortical Impact (CCI) TBI Mouse Model.

All mouse procedures were approved by the University of California San Diego's Institutional Animal Care and Use Committee (IACUC). A total of 61 8–13 week old female C57BL/6J mice (Jackson Labs) weighing between 18–22 g were used for all *in vivo* studies. Following anesthetization with 2.5% isoflurane, buprenorphine analgesia was administered. A 5 mm craniotomy was performed over the right hemisphere between bregma and lambda and controlled cortical impact was performed using the ImpactOne (Leica Biosystems) with a 2 mm diameter stainless steel probe at a velocity of 3 m/s, depth of 2 mm, and dwell time of 300 ms. The center of the injury impact was centered around −2.0 mm (± 0.5 mm) lateral from the midline and −2.0 mm (±0.5 mm) caudal from bregma. Group sizes were n = 3 for each experiment unless noted, based on a type I error rate of 5% and a power of 80% with an anticipated effect size greater than 2 with a 50% variance.

Extracellular Matrix (ECM) Peptide *in Vivo* Screen.

Six hours after CCI, 25 nmoles of ECM-targeting peptide-PEG nanomaterial (quantified *via* FAM absorbance) in 150 μL 5% dextrose was intravenously administered *via* the tail-vein. Nanomaterial doses were administered to mice in a weight range of 18–22 g, corresponding to a dosage range of 1136–1389 nmol/kg. Control cysteine mice received a matching dose as quantified by VivoTag 750 absorbance. Triplicate mice were obtained per ECM-targeting peptide. One hour after injection, mice were transcardially perfused with

USP saline followed by 10% formalin. Surface fluorescence of organs (brain, heart, lung, liver, spleen, kidneys) was measured with an Odyssey scanner (Li-Cor Biosciences) within 6 hours of collection. For generation of tissue for quantitative biodistribution of homogenized tissue, triplicate mice were perfused with 10 mL of ice-cold PBS. For quantification of nanomaterial blood half-life, 5–10 μL of blood was collected into heparinized tubes (n = 3), VivoTag 750 signal was detected on a Li-Cor scanner, and %ID of nanomaterial in the blood was calculated based on a standard of known concentrations and estimated blood volume.

HA-targeted TBI-ABN *in Vivo* Study.

Three hours after CCI, 6 nmoles (concentration based on substrate peptide) of non-targeted, moderate targeting, high targeting TBI-ABN in 150 μL 5% dextrose was injected intravenously *via* the tail vein. Nanomaterial doses were administered to mice with a weight range of 18–22 g, corresponding to a dosage range of 273–333 nmol/kg. Vehicle control received equivolume of 5% dextrose. Following a 1-hour circulation time, mice were sacrificed by transcardial perfusion of either USP saline followed by 10% formalin (for histology) or 10 mL of ice-cold PBS (for whole organ homogenization). Each condition was repeated in triplicate for histology. The study was independently repeated again in triplicate for homogenization tissue generation. A third independent study was performed for CUBIC tissue clearing in one mouse.

Quantitative Biodistribution of Homogenized Tissue.

Organ tissue was flash frozen at −80 °C, tissue was minced, and lysis buffer (6% w/v sodium dodecyl sulfate (SDS), 150 mM Tris-HCl pH 7.4, 100 mM dithiothreitol (DTT), and 2 mM ethylenediaminetetraacetic acid (EDTA)) was added to achieve a concentration of 250 mg tissue/mL. Tissue was further processed with a Tissue-Tearor with 4.5 mm probe (Fisher) at medium-high speed for 20–30 seconds until lysate was homogenized. Samples were heated at 90 °C for 10 minutes with agitation at 800 RPM, vortexed to mix, and homogenate measured for FAM fluorescence (ECM-targeting peptide screen) or Cy5 fluorescence (TBI-ABN activation). Percent injected dose (% ID) per gram of tissue was calculated based on a known nanomaterial concentration standard.

Immunostaining of Brain Tissue Slices.

Following transcardial perfusion with 10% formalin, necropsied organs were further fixed in 10% formalin at 4 °C overnight. Organs were washed in PBS, transferred to 30% w/v sucrose-PBS overnight, then frozen in OCT (Tissue-Tek). Coronal tissue slices 10 μm thick were obtained within the 2 mm diameter injury region, then stained using conventional protocols. See Table S1 for a list of antibodies and staining reagents. Briefly, tissues were blocked for 1 hour in 2% bovine serum albumin, 5% serum of secondary antibody, and 0.1% Triton X-100. For NeuN staining, blocking buffer included 2μg/mL of donkey anti-mouse Fab. Primary antibody incubations were done in blocking buffer overnight at 4 °C. Secondary antibodies were applied for 1 hour at room temperature, washed in PBS, and mounted with Fluoromount-G (Southern Biotech). To probe for endogenous hyaluronic acid, tissues were blocked for 1 hour, incubated overnight with biotinylated hyaluronic acid binding protein (bHABP), incubated for 1 hour with streptavidin AF647 conjugate, washed and mounted. Images were collected on a Nikon Eclipse Ti2 microscope fitted

with a Hamamatsu Orca-Flash 4.0 digital camera. Activated TBI-ABN was visualized with imaging settings for Cy5. Images for direct comparison were collected using the same exposure and LED intensity settings.

In Vitro Reaction Kinetics Assay.

The calpain-1 reaction kinetics assay was run as previously described.[10] Briefly, conjugates were incubated with 26.6 nM human calpain-1 (Sigma-Aldrich, C6108) in 50 mM N-(2-hydroxyethyl)piperazine-N′-ethanesulfonic acid (HEPES), 50 mM NaCl, 2 mM EDTA, 5 mM $CaCl_2$, and 5 mM β-mercaptoethanol. Fluorescence readings were taken every 90 s at 37 °C for 1 h. Reaction curves were normalized to controls, and their initial velocities were fitted to a Michaelis–Menten curve in GraphPad Prism (9.2.0).

CUBIC tissue clearing.

Brains were cleared following published protocol (Clear, Unobstructed Brain/Body Imaging Cocktails and Computational Analysis or CUBIC).[68] Following transcardial perfusion with 10% formalin, the simple immersion protocol for dissected whole brain tissue was followed without modifications. Tissues were kept static in fresh reagent-2 at room temperature between clearing and imaging, with no longer than 1–1.5 weeks between the last day of clearing and imaging.

3D light sheet fluorescence microscopy (LSFM).

Light Sheet Fluorescence Microscopy (LSFM) was accomplished using a Zeiss Lightsheet Z.1. The microscope was fitted with a 2.5x objective, solid-state lasers (excitation wavelengths 488 nm for FAM and 640 nm for sensor) and a PCO.edge 16 bit sCMOS camera for detection. The cleared brain was embedded in low melt 2% agarose (ThermoFisher) then submerged in CUBIC reagent-2 overnight. The next day, magnetic staples were superglued to the agarose-embedded tissue and the sample was hung vertically in front of the LSFM objective (2.5x) using a custom magnetic fixture. The brain was slowly lowered into the imaging chamber filled with reagent-2 for at least 20 minutes prior to image collection. A z-stack (range of 3.258 mm with a 3 μm step size) was obtained. The 3D area, encompassing the injured and contralateral hemispheres, was approximately 9.7 mm (x-axis) by 4.5 mm (y-axis) by 3.3 mm (z-axis). 3D images, clipping planes, and videos were generated in Arivis Vision4D®.

Software and Statistics.

GraphPad Prism® (9.2.0) was used to perform statistics. All images were processed in ImageJ (1.53g).

Supplementary Material

Refer to Web version on PubMed Central for supplementary material.

ACKNOWLEDGMENT

R.M.K acknowledges support from the NHLBI training program Integrative Bioengineering of Heart Vessels Blood (T32 HL105373). J.A.K acknowledges support from the National Science Foundation (NSF) Graduate Research

Fellowship Program under Grant No. DGE-1650112. Any opinions, findings, and conclusions or recommendations expressed in this material are those of the authors and do not necessarily reflect the views of the NSF. We also thank the University of California San Diego School of Medicine microscopy core for use of their light sheet microscopy imaging facilities, supported under NINDS P30NS047101.

Funding Sources

This work was supported by the National Institutes of Health Director's New Innovator Award (1DP2NS111507) and a National Science Foundation (NSF) CAREER Award (CBET 2046926).

REFERENCES

(1). Peterson AB; Zhou H; Thomas K; Daugherty J Surveillance Report of Traumatic Brain Injury-Related Hospitalizations and Deaths by Age Group, Sex, and Mechanism of Injury—United States, 2016 and 2017. Centers Dis. Control Prev 2021.

(2). Maas AIR; Menon DK; Adelson PD; Andelic N; Bell MJ; Belli A; Bragge P; Brazinova A; Büki A; Chesnut RM; Citerio G; Coburn M; Cooper DJ; Crowder AT; Czeiter E; Czosnyka M; Diaz-arrastia R; Gruen RL; Gupta D; Hartings JA; et al. Traumatic Brain Injury : Integrated Approaches to Improve Prevention, Clinical Care, and Research. Lancet Neurol. Comm 2017, 16. DOI: 10.1016/S1474-4422(17)30371-X.

(3). Kandell RM; Waggoner LE; Kwon EJ Nanomedicine for Acute Brain Injuries: Insight from Decades of Cancer Nanomedicine. Mol. Pharm 2020, 18 (2), 522–538. DOI: 10.1021/acs.molpharmaceut.0c00287. [PubMed: 32584042]

(4). Zhang Z; Larner SF; Liu MC; Zheng W; Hayes RL; Wang KKW Multiple AlphaII-Spectrin Breakdown Products Distinguish Calpain and Caspase Dominated Necrotic and Apoptotic Cell Death Pathways. Apoptosis 2009, 14 (11), 1289–1298. DOI: 10.1007/s10495-009-0405-z. [PubMed: 19771521]

(5). Gan ZS; Stein SC; Swanson R; Guan S; Garcia L; Mehta D; Smith DH Blood Biomarkers for Traumatic Brain Injury: A Quantitative Assessment of Diagnostic and Prognostic Accuracy. Front. Neurol 2019, 10, 1–14. DOI: 10.3389/fneur.2019.00446. [PubMed: 30761061]

(6). Siman R; Shahim P; Tegner Y; Blennow K; Zetterberg H; Smith DH Serum SNTF Increases in Concussed Professional Ice Hockey Players and Relates to the Severity of Postconcussion Symptoms. J. Neurotrauma 2015, 32 (17), 1294–1300. DOI: 10.1089/neu.2014.3698. [PubMed: 25419578]

(7). Siman R; Giovannone N; Hanten G; Wilde EA; McCauley SR; Hunter JV; Li X; Levin HS; Smith DH Evidence That the Blood Biomarker SNTF Predicts Brain Imaging Changes and Persistent Cognitive Dysfunction in Mild TBI Patients. Front. Neurol 2013, 4, 190. DOI: 10.3389/fneur.2013.00190. [PubMed: 24302918]

(8). Dudani JS; Warren AD; Bhatia SN Harnessing Protease Activity to Improve Cancer Care. Annu. Rev. Cancer Biol 2018, 2, 353–376. DOI: 10.1146/annurev-cancerbio-030617-050549.

(9). Sanman LE; Bogyo M Activity-Based Profiling of Proteases. Annu. Rev. Biochem 2014, 83, 249–273. DOI: 10.1146/annurev-biochem-060713-035352. [PubMed: 24905783]

(10). Kudryashev JA; Waggoner LE; Leng HT; Mininni NH; Kwon EJ An Activity-Based Nanosensor for Traumatic Brain Injury. ACS Sensors 2020, 5, 686–692. DOI: 10.1021/acssensors.9b01812. [PubMed: 32100994]

(11). Bharadwaj VN; Lifshitz J; Adelson PD; Kodibagkar VD; Stabenfeldt SE Temporal Assessment of Nanoparticle Accumulation after Experimental Brain Injury : Effect of Particle Size. Nat. Sci. Reports 2016, 6, 1–12. DOI: 10.1038/srep29988.

(12). Boyd BJ; Galle A; Daglas M; Rosenfeld JV; Medcalf R Traumatic Brain Injury Opens Blood-Brain Barrier to Stealth Liposomes via an Enhanced Permeability and Retention (EPR)-like Effect. J. Drug Target 2015, 23 (9), 847–853. DOI: 10.3109/1061186X.2015.1034280. [PubMed: 26079716]

(13). Matsumura Y; Maeda H A New Concept for Macromolecular Therapeutics in Cancer Chemotherapy: Mechanism of Tumoritropic Accumulation of Proteins and the Antitumor Agent Smancs. Cancer Res 1986, 46 (8), 6387–6392. [PubMed: 2946403]

(14). Fang J; Nakamura H; Maeda H The EPR Effect: Unique Features of Tumor Blood Vessels for Drug Delivery, Factors Involved, and Limitations and Augmentation of the Effect. Adv. Drug Deliv. Rev 2011, 63 (3), 136–151. DOI: 10.1016/j.addr.2010.04.009. [PubMed: 20441782]

(15). Prasad LK; O'Mary H; Cui Z Nanomedicine Delivers Promising Treatments for Rheumatoid Arthritis. Nanomedicine (Lond) 2015, 10 (13), 2063–2074. DOI: 10.2217/nnm.15.45.Nanomedicine. [PubMed: 26084368]

(16). Horwitz LD; Kaufman D; Keller MW; Kong Y Time Course of Coronary Endothelial Healing after Injury Due to Ischemia and Reperfusion. Circulation 1994, 90 (5), 2439–2447. DOI: 10.1161/01.CIR.90.5.2439. [PubMed: 7955201]

(17). Prajnamitra RP; Chen HC; Lin CJ; Chen LL; Hsieh PCH Nanotechnology Approaches in Tackling Cardiovascular Diseases. Molecules 2019, 24 (10). DOI: 10.3390/molecules24102017.

(18). Kwon EJ; Skalak M; Bu R. Lo; Bhatia SN Neuron-Targeted Nanoparticle for SiRNA Delivery to Traumatic Brain Injuries. ACS Nano 2016, 10, 7926–7933. DOI: 10.1021/acsnano.6b03858. [PubMed: 27429164]

(19). Thorne RG; Nicholson C *In Vivo* Diffusion Analysis with Quantum Dots and Dextrans Predicts the Width of Brain Extracellular Space. Proc. Natl. Acad. Sci. U. S. A 2006, 103 (14), 5567–5572. DOI: 10.1073/pnas.0509425103. [PubMed: 16567637]

(20). Kwon EJ; Dudani JS; Bhatia SN Ultrasensitive Tumour-Penetrating Nanosensors of Protease Activity. Nat. Biomed. Eng 2017, 1 (4). DOI: 10.1038/s41551-017-0054.

(21). Bartlett DW; Su H; Hildebrandt IJ; Weber WA; Davis ME Impact of Tumor-Specific Targeting on the Biodistribution and Efficacy of SiRNA Nanoparticles Measured by Multimodality *in Vivo* Imaging. Proc. Natl. Acad. Sci. U. S. A 2007, 104 (39), 15549–15554. DOI: 10.1073/pnas.0707461104. [PubMed: 17875985]

(22). Choi CHJ; Alabi CA; Webster P; Davis ME Mechanism of Active Targeting in Solid Tumors with Transferrin-Containing Gold Nanoparticles. Proc. Natl. Acad. Sci. U. S. A 2010, 107 (3), 1235–1240. DOI: 10.1073/pnas.0914140107. [PubMed: 20080552]

(23). Park JW; Hong K; Kirpotin DB; Colbern G; Shalaby R; Baselga J; Shao Y; Nielsen UB; Marks JD; Moore D; Papahadjopoulos D; Benz CC Anti-HER2 Immunoliposomes: Enhanced Efficacy Attributable to Targeted Delivery. Clin. Cancer Res 2002, 8 (4), 1172–1181.

(24). Kirpotin DB; Drummond DC; Shao Y; Shalaby MR; Hong K; Nielsen UB; Marks JD; Benz CC; Park JW Antibody Targeting of Long-Circulating Lipidic Nanoparticles Does Not Increase Tumor Localization but Does Increase Internalization in Animal Models. Cancer Res 2006, 66 (13), 6732–6740. DOI: 10.1158/0008-5472.CAN-05-4199. [PubMed: 16818648]

(25). Joo J; Kwon EJ; Kang J; Skalak M; Anglin EJ; Mann AP; Ruoslahti E; Bhatia SN; Sailor MJ Porous Silicon – Graphene Oxide Core-Shell Nanoparticles for Targeted Delivery of SiRNA to the Injured Brain. R. Soc. Chem 2016, 1, 407–414. DOI: 10.1039/c6nh00082g.

(26). Lo JH; Kwon EJ; Zhang AQ; Singhal P; Bhatia SN Comparison of Modular PEG Incorporation Strategies for Stabilization of Peptide-SiRNA Nanocomplexes. Bioconjug. Chem 2016, 27 (10), 2323–2331. DOI: 10.1021/acs.bioconjchem.6b00304. [PubMed: 27583545]

(27). Lin KY; Kwon EJ; Lo JH; Bhatia SN Drug-Induced Amplification of Nanoparticle Targeting to Tumors. Nano Today 2014, 9 (5), 550–559. DOI: 10.1016/j.nantod.2014.09.001. [PubMed: 29731806]

(28). Frantz C; Stewart KM; Weaver VM The Extracellular Matrix at a Glance. J. Cell Sci 2010, 123 (24), 4195–4200. DOI: 10.1242/jcs.023820. [PubMed: 21123617]

(29). Zhang B; Shen S; Liao Z; Shi W; Wang Y; Zhao J; Hu Y; Yang J; Chen J; Mei H; Hu Y; Pang Z; Jiang X Targeting Fibronectins of Glioma Extracellular Matrix by CLT1 Peptide-Conjugated Nanoparticles. Biomaterials 2014, 35 (13), 4088–4098. DOI: 10.1016/j.biomaterials.2014.01.046. [PubMed: 24513320]

(30). Briquez PS; Hauert S; de Titta A; Gray LT; Alpar AT; Swartz MA; Hubbell JA Engineering Targeting Materials for Therapeutic Cancer Vaccines. Front. Bioeng. Biotechnol 2020, 8 (2), 1–26. DOI: 10.3389/fbioe.2020.00019. [PubMed: 32039188]

(31). Ishihara J; Ishihara A; Sasaki K; Hubbell JA Targeted Antibody and Cytokine Cancer Immunotherapies through Collagen Binding. Sci Transl Med 2019, 11 (487). DOI: 10.1016/j.physbeh.2017.03.040.

(32). Williford JM; Ishihara J; Ishihara A; Mansurov A; Hosseinchi P; Marchell TM; Potin L; Swartz MA; Hubbell JA Recruitment of CD103+ Dendritic Cells via Tumor-Targeted Chemokine Delivery Enhances Efficacy of Checkpoint Inhibitor Immunotherapy. Sci. Adv 2019, 5 (12), 0–16. DOI: 10.1126/sciadv.aay1357.

(33). Katsumata K; Ishihara J; Mansurov A; Ishihara A; Raczy MM; Yuba E; Hubbell JA Targeting Inflammatory Sites through Collagen Affinity Enhances the Therapeutic Efficacy of Anti-Inflammatory Antibodies. Sci. Adv 2019, 5, 1–9. DOI: 10.1126/sciadv.aay1971.

(34). Katsumata K; Ishihara J; Fukunaga K; Ishihara A; Yuba E; Budina E; Hubbell JA Conferring Extracellular Matrix Affinity Enhances Local Therapeutic Efficacy of Anti-TNF-α Antibody in a Murine Model of Rheumatoid Arthritis. Arthritis Res. Ther 2019, 21 (1), 1–10. DOI: 10.1186/s13075-019-2075-8. [PubMed: 30606217]

(35). Price L; Wilson C; Grant G Chapter 4: Blood – Brain Barrier Pathophysiology Following Traumatic Brain Injury. In Translational Research in Traumatic Brain Injury; Laskowitz D, Grant G, Eds.; CRC Press/Taylor and Francis Group: Boca Raton, 2016; pp 1–10.

(36). George N; Geller H Extracellular Matrix and Traumatic Brain Injury. J. Neurosci 2018, 96 (4), 573–588. DOI: 10.1002/jnr.24151.Extracellular.

(37). Lau LW; Cua R; Keough MB; Haylock-Jacobs S; Yong VW Pathophysiology of the Brain Extracellular Matrix: A New Target for Remyelination. Nat. Rev. Neurosci 2013, 14 (10), 722–729. DOI: 10.1038/nrn3550. [PubMed: 23985834]

(38). Xing G; Ren M; Verma A Divergent Temporal Expression of Hyaluronan Metabolizing Enzymes and Receptors with Craniotomy *vs.* Controlled-Cortical Impact Injury in Rat Brain: A Pilot Study. Front. Neurol 2014, 5 (9), 1–9. DOI: 10.3389/fneur.2014.00173. [PubMed: 24454306]

(39). Mann AP; Scodeller P; Hussain S; Joo J; Kwon E; Braun GB; Molder T; She Z; Kotamraju VR; Ranscht B; Krajewski S; Teesalu T; Bhatia SN; Sailor M; Ruoslahti E A Peptide for Targeted, Systemic Delivery of Imaging and Therapeutic Compounds into Acute Brain Injuries. Nat. Commun 2016, 7, 1–11. DOI: 10.1038/ncomms11980.

(40). Chan JM; Zhang L; Tong R; Ghosh D; Gao W; Liao G; Yuet KP; Gray D; Rhee JW; Cheng J; Golomb G; Libby P; Langer R; Farokhzad OC Spatiotemporal Controlled Delivery of Nanoparticles to Injured Vasculature. Proc. Natl. Acad. Sci. U. S. A 2010, 107 (5), 2213–2218. DOI: 10.1073/pnas.0914585107. [PubMed: 20133865]

(41). Simberg D; Duza T; Park JH; Essler M; Pilch J; Zhang L; Derfus AM; Yang M; Hoffman RM; Bhatia S; Sailor MJ; Ruoslahti E Biomimetic Amplification of Nanoparticle Homing to Tumors. Proc. Natl. Acad. Sci. U. S. A 2007, 104 (3), 932–936. DOI: 10.1073/pnas.0610298104. [PubMed: 17215365]

(42). Tolg C; Hamilton SR; Zalinska E; McCulloch L; Amin R; Akentieva N; Winnik F; Savani R; Bagli DJ; Luyt LG; Cowman MK; McCarthy JB; Turley EA A RHAMM Mimetic Peptide Blocks Hyaluronan Signaling and Reduces Inflammation and Fibrogenesis in Excisional Skin Wounds. Am. J. Pathol 2012, 181 (4), 1250–1270. DOI: 10.1016/j.ajpath.2012.06.036. [PubMed: 22889846]

(43). Faust HJ; Sommerfeld SD; Rathod S; Rittenbach A; Ray Banerjee S; Tsui BMW; Pomper M; Amzel ML; Singh A; Elisseeff JH A Hyaluronic Acid Binding Peptide-Polymer System for Treating Osteoarthritis. Biomaterials 2018, 183 (August), 93–101. DOI: 10.1016/j.biomaterials.2018.08.045. [PubMed: 30149233]

(44). Waggoner LE; Madias MI; Hurtado AA; Kwon EJ Pharmacokinetic Analysis of Peptide-Modified Nanoparticles with Engineered Physicochemical Properties in a Mouse Model of Traumatic Brain Injury. AAPS J 2021, 23 (100), 1–12. DOI: 10.1208/s12248-021-00626-5.

(45). Choi HS; Liu W; Misra P; Tanaka E; Zimmer JP; Itty Ipe B; Bawendi MG; Frangioni JV Renal Clearance of Nanoparticles. Nat. Biotechnol 2009, 25 (10), 1165–1170. DOI: 10.1038/nbt1340.Renal.

(46). Nance EA; Woodworth GF; Sailor KA; Shih TY; Xu Q; Swaminathan G; Xiang D; Eberhart C; Hanes J A Dense Poly(ethylene Glycol) Coating Improves Penetration of Large Polymeric Nanoparticles within Brain Tissue. Sci. Transl. Med 2012, 4 (149). DOI: 10.1126/scitranslmed.3003594.

(47). Suk JS; Xu Q; Kim N; Hanes J; Ensign L PEGylation as a Strategy for Improving Nanoparticle-Based Drug and Gene Delivery. Adv Drug Deliv. Rev 2016, 99 (Pt A), 28–51. DOI: 10.1016/j.addr.2015.09.012.PEGylation. [PubMed: 26456916]

(48). Pierschbacher MD; Ruoslahti E Cell Attachment Activity of Fibronectin Can Be Duplicated By Small Synthetic Fragments of the Molecule. Nature 1984, 3–6.

(49). Mezu-Ndubuisi OJ; Maheshwari A The Role of Integrins in Inflammation and Angiogenesis. Pediatr. Res 2021, 89 (7), 1619–1626. DOI: 10.1038/s41390-020-01177-9. [PubMed: 33027803]

(50). Abumiya T; Lucero J; Heo JH; Tagaya M; Koziol JA; Copeland BR; Del Zoppo GJ Activated Microvessels Express Vascular Endothelial Growth Factor and Integrin α(v)B3 during Focal Cerebral Ischemia. J. Cereb. Blood Flow Metab 1999, 19 (9), 1038–1050. DOI: 10.1097/00004647-199909000-00012. [PubMed: 10478656]

(51). Ward PA Inflammation and α vβ 3 Integrin. Am. J. Respir. Crit. Care Med 2012, 185 (1), 5–6. DOI: 10.1164/rccm.201110-1859ED. [PubMed: 22210783]

(52). Xiong Y; Mahmood A; Chopp M Animal Models of Traumatic Brain Injury. Nat. Rev. Neurosci 2013, 14 (2), 128–142. DOI: 10.1038/nrn3407. [PubMed: 23329160]

(53). Hall ED; Sullivan PG; Gibson TR; Pavel KM; Thompson BM; Scheff SW Spatial and Temporal Characteristics of Neurodegeneration after Controlled Cortical Impact in Mice: More Than a Focal Brain Injury. J. Neurotrauma 2005, 22 (2), 252–265. DOI: 10.1089/neu.2005.22.252. [PubMed: 15716631]

(54). Natarajan V; Harris EN; Kidambi S SECs (Sinusoidal Endothelial Cells), Liver Microenvironment, and Fibrosis. Biomed Res. Int 2017, 4097205, 1–9. DOI: 10.1155/2017/4097205.

(55). Perrault SD; Walkey C; Jennings T; Fischer HC; Chan WCW Mediating Tumor Targeting Efficiency of Nanoparticles through Design. Nano Lett 2009, 9 (5), 1909–1915. DOI: 10.1021/nl900031y. [PubMed: 19344179]

(56). Hamakubo T; Kannagi R; Murachi T; Matus A Distribution of Calpains I and II in Rat Brain. J. Neurosci 1986, 6 (11), 3103–3111. DOI: 10.1523/jneurosci.06-11-03103.1986. [PubMed: 3021924]

(57). Czogalla A; Sikorski AF Spectrin and Calpain: A “Target” and a “Sniper” in the Pathology of Neuronal Cells. Cell. Mol. Life Sci 2005, 62 (17), 1913–1924. DOI: 10.1007/s00018-005-5097-0. [PubMed: 15990959]

(58). Xiong Y; Mahmood A; Chopp M Emerging Treatments for Traumatic Brain Injury. Expert Opin. Emerg. Drugs 2009, 14 (1), 67–84. DOI: 10.1517/14728210902769601. [PubMed: 19249984]

(59). Heinegard D; Hascall VC Aggregation of Cartilage Proteoglycans III. Characteristics of the Proteins Isolated from Trypsin Digests of Aggregates. J. Biol. Chem 1974, 249 (13), 4232–4241. DOI: 10.1016/S0021-9258(19)42509-X. [PubMed: 4277351]

(60). Ueno H; Suemitsu S; Murakami S; Kitamura N; Wani K; Matsumoto Y; Aoki S; Okamoto M; Ishihara T Hyaluronic Acid Is Present on Specific Perineuronal Nets in the Mouse Cerebral Cortex. Brain Res 2018, 1698 (August), 139–150. DOI: 10.1016/j.brainres.2018.08.011. [PubMed: 30099038]

(61). Arranz AM; Perkins KL; Irie F; Lewis DP; Hrabe J; Xiao F; Itano N; Kimata K; Hrabetova S; Yamaguchi Y Hyaluronan Deficiency Due to Has3 Knock-Out Causes Altered Neuronal Activity and Seizures *via* Reduction in Brain Extracellular Space. J. Neurosci 2014, 34 (18), 6164–6176. DOI: 10.1523/JNEUROSCI.3458-13.2014. [PubMed: 24790187]

(62). Kochlamazashvili G; Henneberger C; Bukalo O; Senkov O; Lievens PM; Westenbroek R; Andreas K; Catterall WA; Rusakov DA; Schachner M The Extracellular Matrix Molecule Hyaluronic Acid Regulates Hippocampal Synaptic Plasticity by Modulating Postsynaptic L-Type Ca 2 + Channels. Neuron 2012, 67 (1), 116–128. DOI: 10.1016/j.neuron.2010.05.030.The.

(63). Stockholm D; Bartoli M; Sillon G; Bourg N; Davoust J; Richard I Imaging Calpain Protease Activity by Multiphoton FRET in Living Mice. J. Mol. Biol 2005, 346 (1), 215–222. DOI: 10.1016/j.jmb.2004.11.039. [PubMed: 15663939]

(64). Jeong W. jin; Bu J; Kubiatowicz LJ; Chen SS; Kim YS; Hong S Peptide–Nanoparticle Conjugates: A Next Generation of Diagnostic and Therapeutic Platforms? Nano Converg 2018, 5 (1), 1–18. DOI: 10.1186/s40580-018-0170-1. [PubMed: 29375956]

(65). Vindis C; Elbaz M; Escargueil-Blanc I; Auge N; Heniquez A; Thiers JC; Nègre-Salvayre A; Salvayre R Two Distinct Calcium-Dependent Mitochondrial Pathways Are Involved in Oxidized LDL-Induced Apoptosis. Arterioscler. Thromb. Vasc. Biol 2005, 25 (3), 639–645. DOI: 10.1161/01.ATV.0000154359.60886.33. [PubMed: 15618541]

(66). Smith MA; Schnellmann RG Calpains, Mitochondria, and Apoptosis. Cardiovasc. Res 2012, 96 (1), 32–37. DOI: 10.1093/cvr/cvs163. [PubMed: 22581845]

(67). Chen YC; Mao H; Yang KH; Abel T; Meaney DF A Modified Controlled Cortical Impact Technique to Model Mild Traumatic Brain Injury Mechanics in Mice. Front. Neurol 2014, 5 JUN (6), 1–14. DOI: 10.3389/fneur.2014.00100. [PubMed: 24454306]

(68). Susaki EA; Tainaka K; Perrin D; Yukinaga H; Kuno A; Ueda HR Advanced CUBIC Protocols for Whole-Brain and Whole-Body Clearing and Imaging. Nat. Protoc 2015, 10 (11), 1709–1727. DOI: 10.1038/nprot.2015.085. [PubMed: 26448360]

(69). Kirkpatrick JD; Warren AD; Soleimany AP; Westcott PMK; Voog JC; Martin-Alonso C; Fleming HE; Tammela T; Jacks T; Bhatia SN Urinary Detection of Lung Cancer in Mice via Noninvasive Pulmonary Protease Profiling. Sci. Transl. Med 2020, 12, 1–10. DOI: 10.1126/scitranslmed.aaw0262.

(70). Dudani JS; Ibrahim M; Kirkpatrick J; Warren AD; Bhatia SN Classification of Prostate Cancer Using a Protease Activity Nanosensor Library. Proc. Natl. Acad. Sci. U. S. A 2018, 115 (36), 8954–8959. DOI: 10.1073/pnas.1805337115. [PubMed: 30126988]

(71). Guilfoyle MR; Carpenter KLH; Helmy A; Pickard JD; Menon DK; Hutchinson PJA Matrix Metalloproteinase Expression in Contusional Traumatic Brain Injury: A Paired Microdialysis Study. J. Neurotrauma 2015, 32 (20), 1553–1559. DOI: 10.1089/neu.2014.3764. [PubMed: 25858502]

(72). Knopp RC; Jastaniah A; Dubrovskyi O; Gaisina I; Tai L; Thatcher GRJ Extending the Calpain-Cathepsin Hypothesis to the Neurovasculature: Protection of Brain Endothelial Cells and Mice from Neurotrauma. ACS Pharmacol. Transl. Sci 2021, 4 (1), 372–385. DOI: 10.1021/acsptsci.0c00217. [PubMed: 33615187]

(73). Tsubokawa T; Solaroglu I; Yatsushige H; Cahill J; Yata K; Zhang JH Cathepsin and Calpain Inhibitor E64d Attenuates Matrix Metalloproteinase-9 Activity after Focal Cerebral Ischemia in Rats. Stroke 2006, 37 (7), 1888–1894. DOI: 10.1161/01.STR.0000227259.15506.24. [PubMed: 16763180]

(74). Samanta A; Zhou Y; Zou S; Yan H; Liu Y Fluorescence Quenching of Quantum Dots by Gold Nanoparticles: A Potential Long Range Spectroscopic Ruler. Nano Lett 2014, 14 (9), 5052–5057. DOI: 10.1021/nl501709s. [PubMed: 25084363]

(75). Shin TH; Kang S; Park S; Choi J. sil; Kim PK; Cheon JA Magnetic Resonance Tuning Sensor for the MRI Detection of Biological Targets. Nat. Protoc 2018, 13 (11), 2664–2684. DOI: 10.1038/s41596-018-0057-y. [PubMed: 30349049]

(76). Girgis F; Pace J; Sweet J; Miller JP Hippocampal Neurophysiologic Changes after Mild Traumatic Brain Injury and Potential Neuromodulation Treatment Approaches. Front. Syst. Neurosci 2016, 10 (2), 1–10. DOI: 10.3389/fnsys.2016.00008. [PubMed: 26834579]

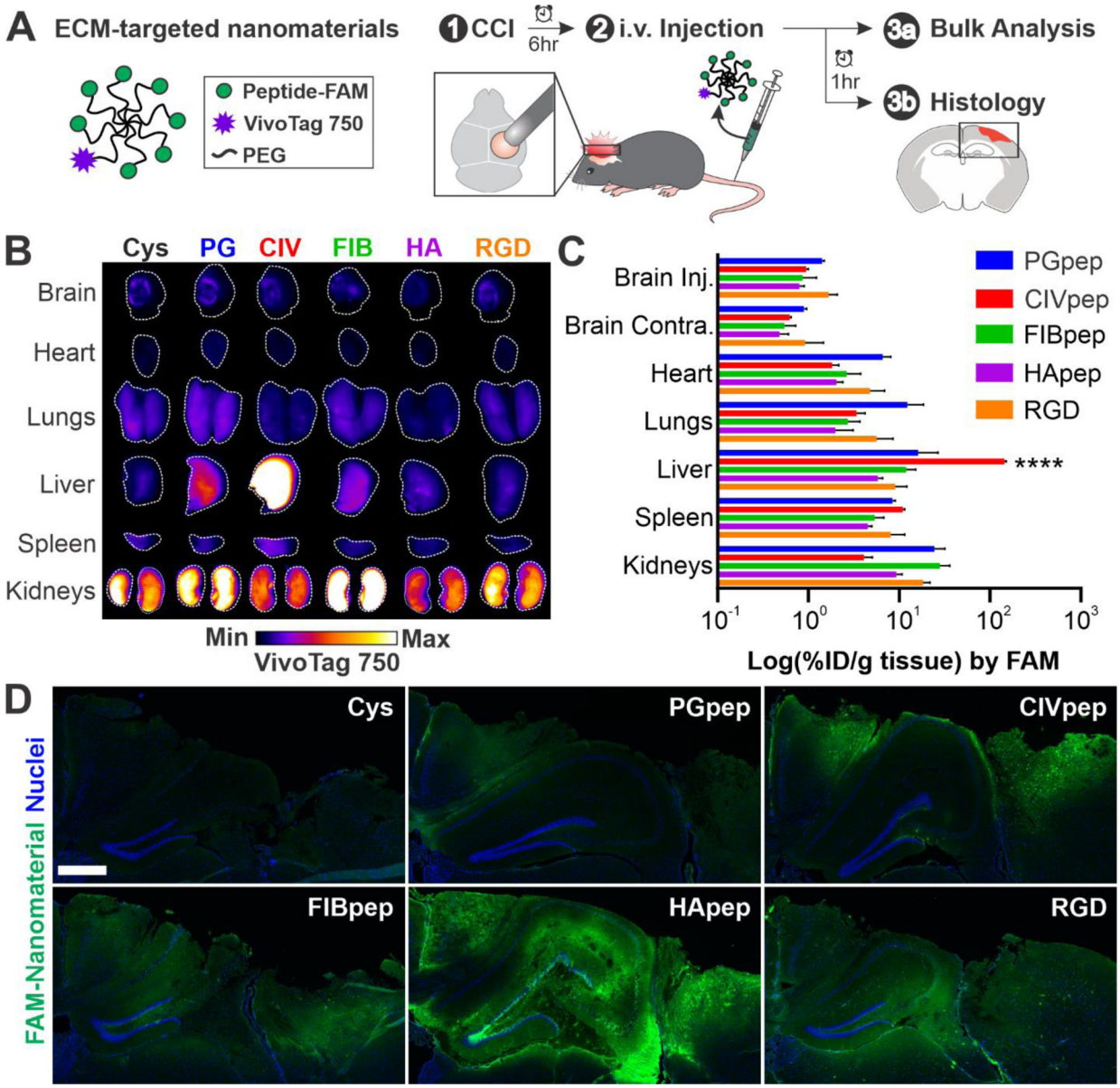

Figure 1.

Nanomaterial modification with HA-targeting peptide leads to widespread distribution in the injured brain after systemic administration. (A) Schematic of ECM-targeted nanomaterials and overview of experimental design. 6 hours post-CCI, ECM-targeted nanomaterials were intravenously administered. After 1 hour, organs were harvested for analysis of nanomaterial biodistribution and histology. (B) Surface imaging of VivoTag 750 from major organs of one representative mouse per nanomaterial (n = 3, white line indicates outline of organ). (C) Bulk quantification of percent injected dose nanomaterial per gram (% ID/g) tissue based on FAM fluorescence (n = 3, mean ± SEM, ****p ≤ 0.0001, two-way ANOVA and Tukey's multiple comparisons post-hoc test within each organ group). (D) Representative images of the injured cortex in coronal brain slices (n = 3; blue, nuclei; green, FAM-labeled ECM-targeting peptide on nanomaterial; scale bar = 500 μm).

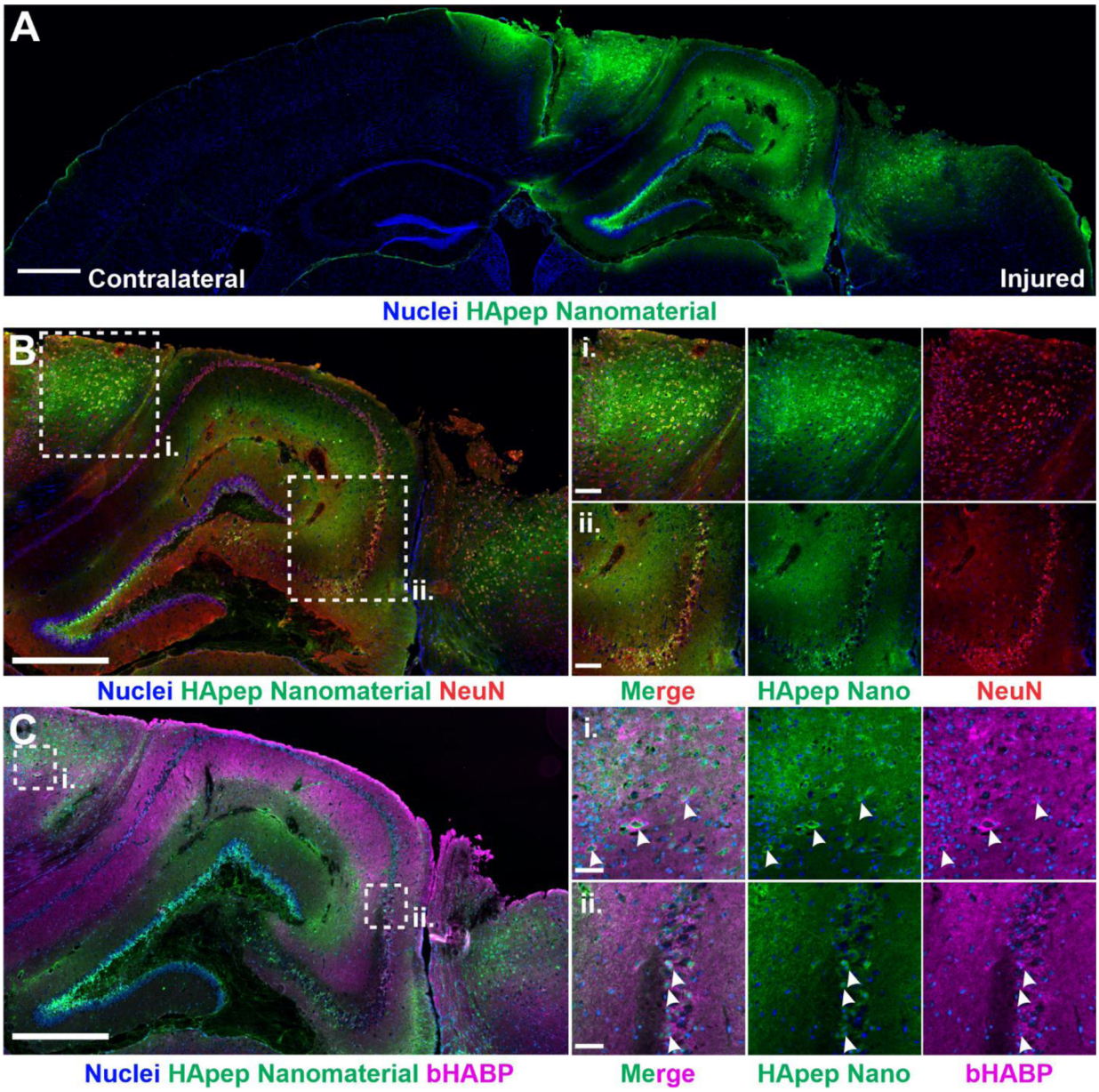

Figure 2.

Hyaluronic acid-targeted nanomaterial distributes across perilesional brain tissue in CCI-injured brains. (A) Coronal brain sections from mice administered i.v. HApep-modified nanomaterial 6 hours post-CCI after 1 hour of circulation (blue, nuclei; green, HApep on nanomaterial; scale bar = 500 μm). (B) HApep-modified nanomaterial in the injured cortex stained for neurons (red, NeuN; scale bar = 500 μm). Insets show (i) perilesional cortex and (ii) hippocampus (scale bar = 100 μm). (C) Injured cortex labeled with biotinylated hyaluronic acid binding protein (magenta, bHABP; scale bar = 500 μm). Insets show (i) perilesional cortex and (ii) hippocampus (scale bar = 50 μm). Arrows note instances of nanomaterial colocalization with HABP staining.

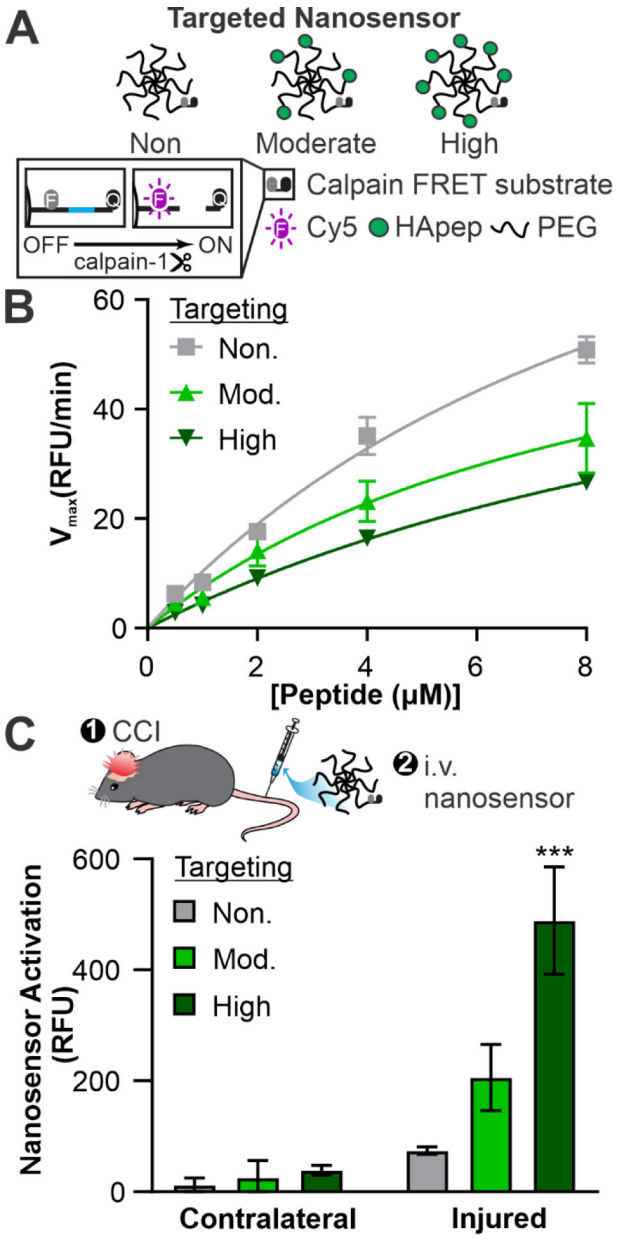

Figure 3.

Hyaluronic acid targeting improves nanosensor signal generation in a CCI mouse model of TBI. (A) Schematic of HApep-modified nanosensors with no, moderate, and high targeting. (B) Michaelis-Menten cleavage kinetics of nanosensors incubated with human calpain-1 (n = 3, mean ± SD). (C) Activated nanosensor signal measured in cortical brain tissue lysate collected from the contralateral and injured hemispheres (n = 3, mean ± SEM, ***$p \leq 0.001$, two-way ANOVA with Sidak's multiple comparisons post-hoc test compared to non-targeted groups).

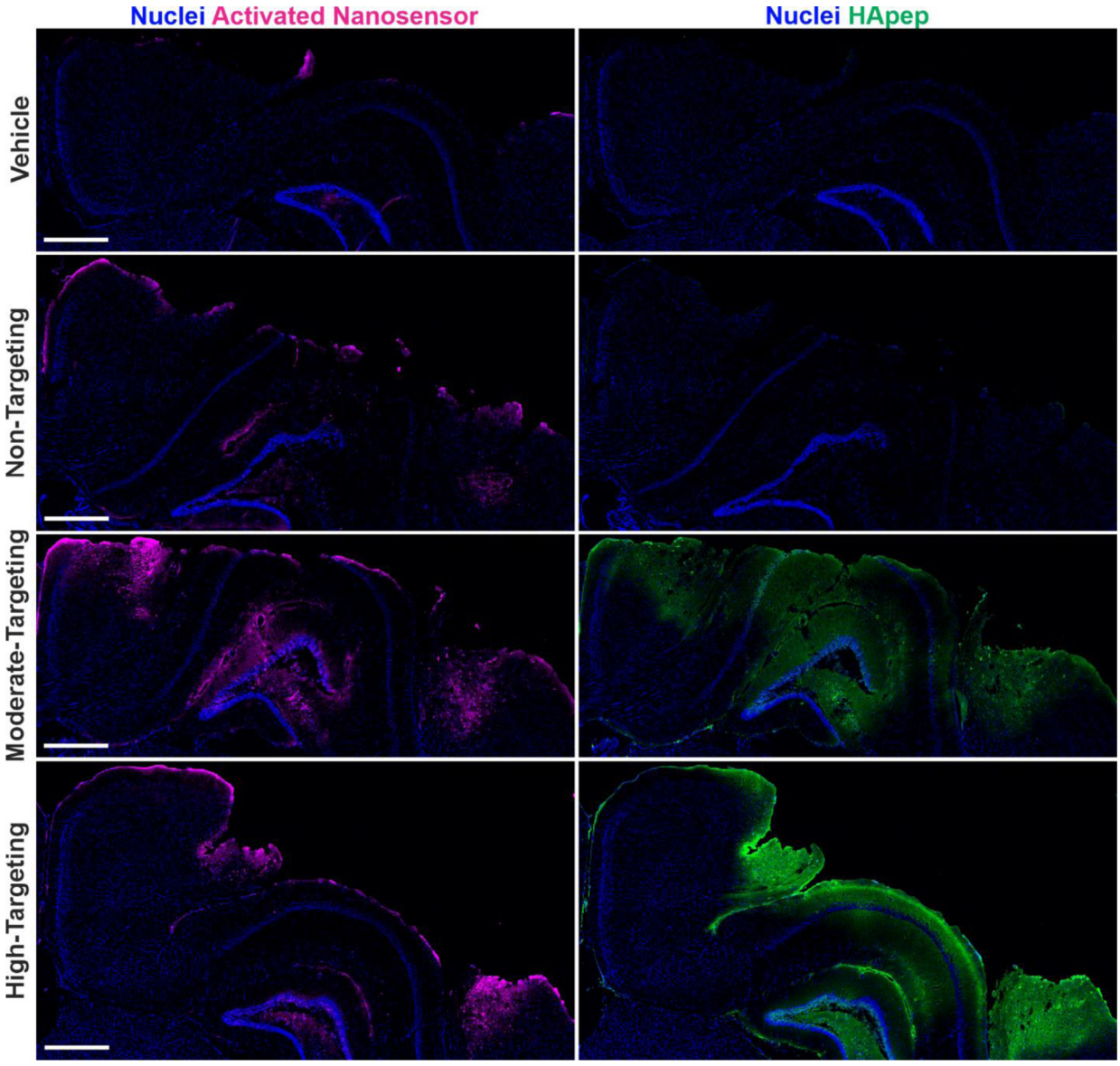

Figure 4.

Hyaluronic acid peptide targeting increases overall TBI-ABN activation and distribution within coronal sections of the injured hemisphere. Injured hemispheres from CCI-injured mice (representative brains from triplicate) after intravenous administration of vehicle or nanosensors with non-, moderate- or high-targeting modification (blue, nuclei; magenta, activated nanosensor; green, HApep on nanosensor; scale bar = 500 μm).

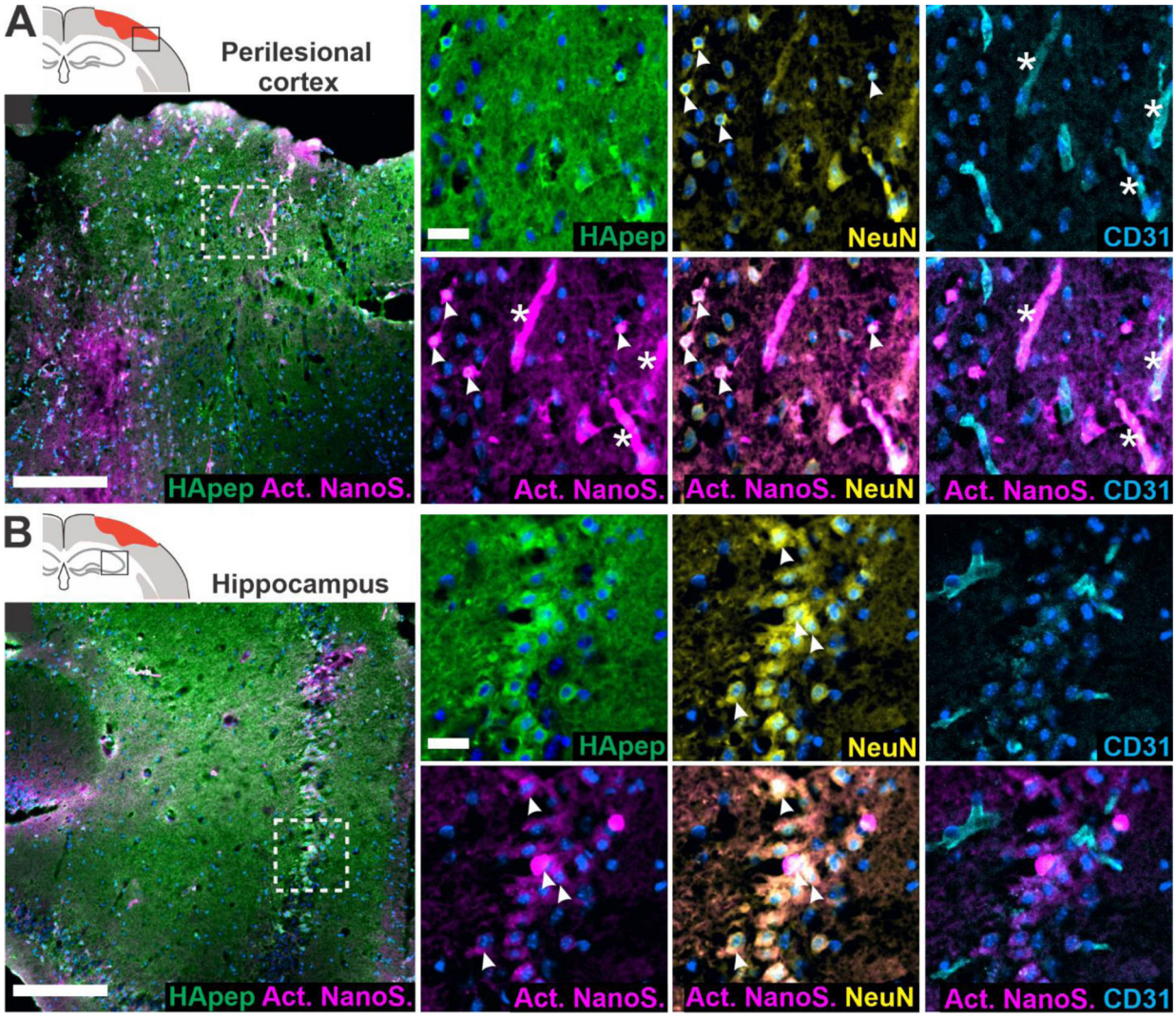

Figure 5.

Hyaluronic acid-targeted nanosensor activates within neuronal and endothelial cells in the perilesional cortex and hippocampus. Images from the (A) perilesional cortex and (B) hippocampus imaged for nanosensor distribution and activated nanosensor (box in schematic indicates imaging location). Immunostaining was performed for HApep (green, FAM), neurons (yellow, NeuN), and endothelial cells (cyan, CD31) (blue, nuclei; magenta, activated nanosensor; scale bar = 200 μm for larger images and 25 μm for insets). Colocalization of nanosensor activation with neurons or endothelial cells are denoted with arrows or stars, respectively.

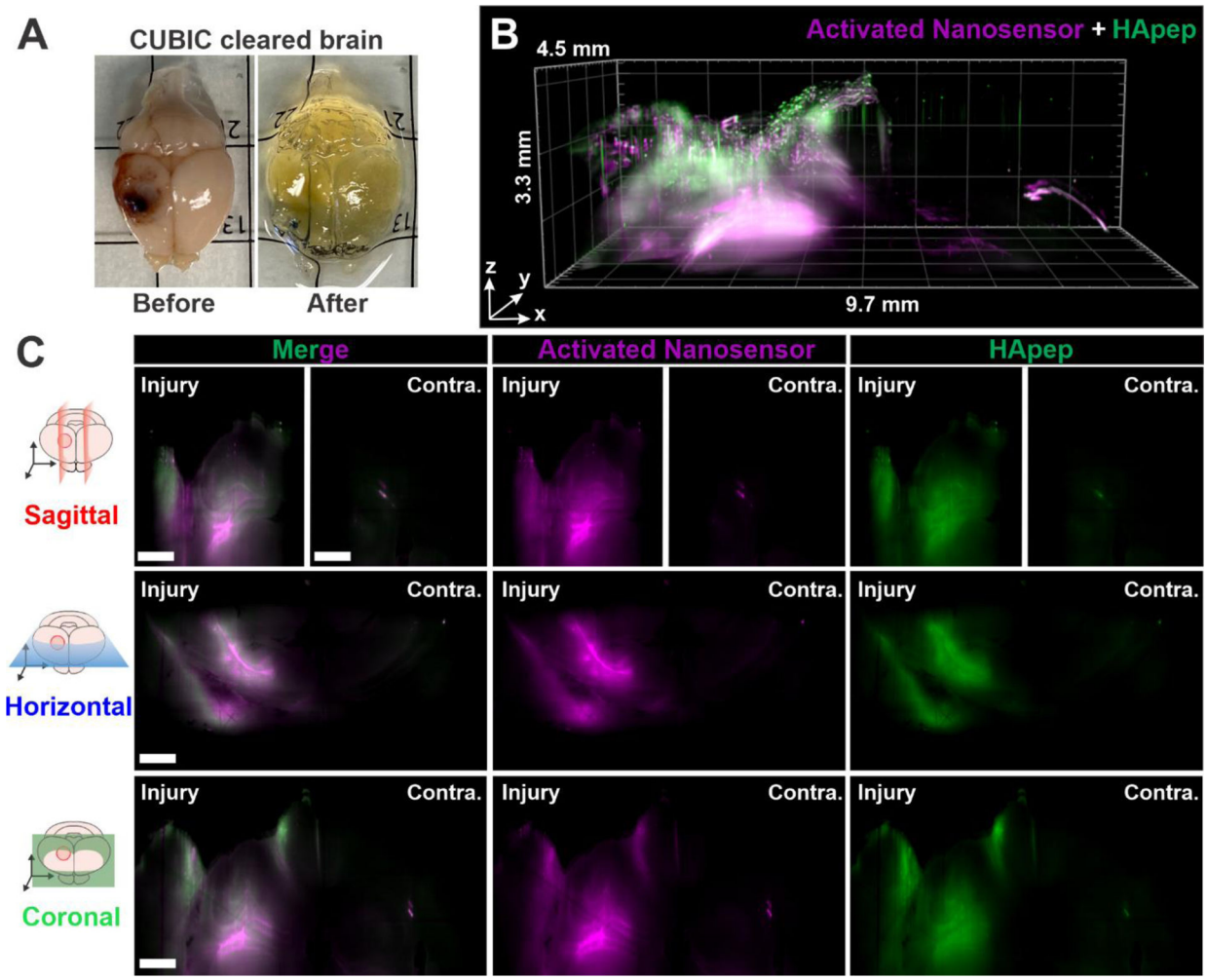

Figure 6.

Light sheet fluorescence microscopy (LSFM) of cleared tissues enables 3-dimensional (3D) reconstruction of nanosensor activation within the injured brain. (A) Image of injured brain before and after whole brain CUBIC clearing. (B) 3D render view. (C) Sagittal, horizontal, and coronal cross sections (magenta, activated nanosensor; green, HApep on nanosensor; scale bar = 1 mm; Contra. = contralateral hemisphere). See Supplementary Video and Supplementary Figure S10 for the clipping planes used to generate the cross-sections.

Table 1.

Brain ECM targeting peptides and their properties.

peptide name	ECM target	peptide sequence	pI[a]	GRAVY[b]
PGpep	proteoglycans	CAQK[39]	9.13	−0.78
CIVpep	collagen IV	KLWVLPK[40]	10.69	0.21
FIBpep	fibrin	CREKA[41]	9.12	−1.52
HApep	hyaluronic acid	STMMSRSHKTRSHHV[42]	12.13	−1.27

[a] pI = isoelectric point

[b] GRAVY = grand average of hydropathy